Ultrasound phased arrays for prostate treatment

Joseph S. Tan and Leon A. Frizzell
Bioacoustics Research Laboratory, Department of Electrical and Computer Engineering, University of Illinois, 405 North Mathews Avenue, Urbana, Illinois 61801

Narendra Sanghvi, Shih-jeh Wu,[a] and Ralf Seip
Focus Surgery, Inc., 3940 Pendleton Way, Indianapolis, Indiana 46226

Jeffrey T. Kouzmanoff[b]
Labthermics Technologies, Inc., 701 Devonshire Drive, Champaign, Illinois 61820

(Received 6 June 2000; accepted for publication 26 March 2001)

The effect of array geometry on the steering performance of ultrasound phased arrays is examined theoretically, in order to maximize array performance under the given anatomical constraints. This paper evaluates the performance of arrays with spherical and cylindrical geometry, determined by using computer simulations of the pressure fields produced at various extremes of steering. The spherical segment arrays were truncated for insertion into the rectum, and contained either annular or linear elements. The cylindrical arrays were either flat or had a variable curvature applied along their length. Fields were computed by dividing the array elements into many point sources. The effectiveness of an array configuration when steered to a particular focal location was assessed by defining a parameter, G, as the ratio of the intensity at the desired focus to the maximum intensity of any unwanted lobes. The performance of truncated spherical arrays with annular elements was evaluated for focal steering along the array axis (in depth, in the z direction). When steered 15 mm toward the source, these truncated spherical annular arrays exhibited excellent performance, with $G>5.7$ for arrays containing more than 10 elements. Similarly, the spherical arrays with linear elements performed well when steered along the array axis to the same degree, with $G>7$ (for element widths up to 3 λ), though many more array elements were required. However, when these arrays were steered 15 mm laterally, along the length of the prostate (the y direction), the value for G fell below 1 for element widths greater than about 1.6 λ. It was found that the cylindrical arrays performed much better for y-direction steering ($G>4$, for 60 mm arrays with an element width of 1.75 λ), but their performance was poorer when steered in the z direction ($G\cong 4$ for an element width of 1.5 λ). In order to find a compromise between these extremes, a curved cylindrical array was examined, which was a cylindrical array with additional curvature along its length. These curved cylindrical arrays yielded performance between that of spherical linear arrays and cylindrical arrays, with better steering along the y direction than the spherical arrays and better z-direction steering than the cylindrical arrays. © *2001 Acoustical Society of America.*
[DOI: 10.1121/1.1373444]

PACS numbers: 43.80.Sh, 43.80.Vj [FD]

I. INTRODUCTION

Two diseases of the prostate, benign prostatic hyperplasia (BPH) and cancer of the prostate (PC), are problems that are increasingly afflicting our male population. The incidence of both conditions increases with age and concern about these diseases is reflected in increased exposure in the popular[1–3] as well as in the medical literature.[4] Current treatment options can be fairly expensive, and are associated with a high incidence of impotence, frequent urinary incontinence, as well as the risks associated with surgical procedures.[5] Since none of these treatment options are ideal, alternative therapies are currently being sought.[1,4–6]

In recent years, ultrasound has been increasingly investigated for use in thermal or ablative therapy.[7–20] When focused, ultrasound can produce well-defined regions of thermal necrosis for treatment of prostate disease.[7,9,19–25] In the treatment of the prostate, focused ultrasound is applied via a probe inserted into the rectum, in order to minimize the amount of intervening tissue while providing an adequate acoustic window for treatment. This allows higher frequencies to be used, increasing the ultrasonic absorption coefficient and resulting in more efficient heating of the treatment region.[15] Additionally, transrectal treatment avoids undesired heating of the pelvic bone. Preliminary findings have demonstrated that ultrasonic ablation can successfully control localized prostate cancer with low morbidity.[19,25] This approach has been shown not to enhance metastatic spread,[26,27] and avoids damage to the rectal wall.[28]

Transrectal ultrasonic therapy of the prostate imposes geometric constraints on the transducer utilized in the treatment, because the ultrasound probe containing the array must fit within the patient's rectum. This limits the practical array

[a]Current address: I-Shou University, Section 1, Hsueh-Cheng Rd., Ta-Hsu Hsiang, Kaohsiung County, Taiwan, 84008, Republic of China.
[b]Current address: Cisco Systems, Inc., 2302 Fox Drive, Champaign, IL 61820.

width. The ability to move the focal point is essential, since the treatment region is larger in volume than the ultrasonic focus. With a steerable focus, the focus can be placed at various locations in a controlled manner, in order to ablate the entire treatment volume.[13,18,29,30] Current devices in clinical trials use a single spherical transducer with a fixed focus.[16,19,20] Variation of the focal position is achieved through mechanical movement of the transducer, and variation of focal depth can only be accomplished by using a different transducer with a different radius of curvature. Because mechanical components are subject to failure due to wear, and because changing transducers requires time both to switch transducers and to reposition the new transducer relative to the prostate, it would be advantageous to employ a phased array transducer system, and steer the focus electronically. The phased array would offer the advantages of steering the focal region very rapidly with minimal mechanical movement of the transducer and the possibility of modifying the focal size by electronic means.[17,30,31] These capabilities would facilitate the efficient treatment of large tumor volumes. The inevitable disadvantages of phased arrays include the need to manufacture arrays with many small, acoustically isolated elements; the associated large number of electrical leads, amplifiers and phasing circuits; and the existence of unwanted lobes, including grating lobes in the field, which might be of sufficient intensity to cause unintended damage to normal tissue. More intense unwanted lobes also result in longer treatment times, as greater waiting periods between sonications are required in order to allow for thermal dissipation, to prevent heat build-up in normal tissue regions.

A number of methods have been investigated in order to improve the performance of surgical phased arrays. These methods have, for the most part, involved modifications occurring at the level of the array elements, for example, element size randomization in linear arrays,[23] adaptive aperture techniques,[32] permutations in element layout,[33,34] or novel phasing schemes.[17,30,31,35] A few have involved the introduction of new phased array shapes, such as spherical-section arrays[36,37] and a cylindrical array.[38] In this theoretical study, a number of transducer array configurations were examined in order to elucidate the effects of array geometry on performance. This was conducted with the intent of determining which of these configurations would be optimal in terms of using the fewest elements while providing acceptable ultrasonic fields and flexible focusing capability for prostate therapy through the rectum. Thus, the goal was not to eliminate unwanted lobes entirely but to insure that they were of acceptably low amplitude while steering the focus over the intended range, so as to minimize unintended heating elsewhere in the field. To this end, only arrays containing element widths larger than a wavelength were examined. Although sparsely filled, randomized spherical arrays have been shown to be highly effective in suppressing unwanted lobes,[11,12,33] the limited surface area available in transrectal prostate therapy precludes the use of a sparsely filled array.

The first transducer array examined was a truncated spherical segment with annular elements for steering the focus in depth along the axis of the transducer. A second spherical array with linear elements was investigated for steering the focus both axially and laterally along the length of the prostate. In order to improve steering along the length of the prostate, a cylindrical array geometry was then examined. Finally, a novel transducer array design was examined, which involved the addition of curvature along the length of the cylindrical array. This curved cylindrical array can be considered a hybrid of the truncated spherical array and the cylindrical array. For array configurations fitting within the geometric constraints mentioned earlier, computational studies were performed, in order to assess their effectiveness in delivering high intensity ultrasonic energy to specified focal positions. The effectiveness of an array configuration when steered to a particular focal location was assessed by defining a parameter, G, as the ratio of the intensity at the desired focus to the maximum intensity of any unwanted lobes. The focal positions employed in the studies correspond to the anticipated steering extremes required during clinical use of the array for prostate therapy.

II. METHODS

The pressure fields produced by the arrays examined in this study were calculated using the point radiator method, which subdivides the elements of the array into subelements that are small enough that they produce fields approximating that from a point radiator.[39–41] The total pressure at any given point in the field is the sum of the complex pressures contributed from each of the subelements across the entire active surface of the array, taking into account the relative phase of the signal applied to the transducer element to which the subelement belongs. The pressure field produced by a given array configuration (geometry, element width and element spacing) could be calculated for the focus steered to any specified location. The origin of the coordinate system was taken as 45 mm from the center of the array with the positive z axis directed away from the array, the y axis was directed along the length of the array and the x axis across the array, as shown in Fig. 1. This point was chosen as the origin because it represents a typical distance between the transducer face located in the rectum and the deepest extent of the treatment region into the prostate. Additionally, the origin corresponds to the geometric focus of the spherical arrays. Signals applied to the elements of the array were phased so as to result in constructive interference at the intended focal point.

The pressure field was calculated at points in the region of interest using the following equation:

$$p(x,y,z) \cong j \frac{\rho c k U_0 \Delta A}{2\pi} \sum_{\text{array surface}} \frac{e^{-(\alpha + jk)R}}{R}, \tag{1}$$

where the summation is over the active surface of the array, i.e., the surface of the elements of the array, $p(x,y,z)$ is the total acoustic pressure at the point (x,y,z), ρ is the density and c is the speed of sound of the loading medium, k is the acoustic propagation constant (calculated from $k=2\pi/\lambda$, where λ is the wavelength), U_0 is the velocity amplitude of the surface of the source in m/s [calculated from $U_0 = (2I_0/\rho c)^{1/2}$, where $I_0 = 10\,000\ \text{W/m}^2$], $R=[(x-x_s)^2+(y-y_s)^2+(z-z_s)^2]^{1/2}$ is the distance from the center of the

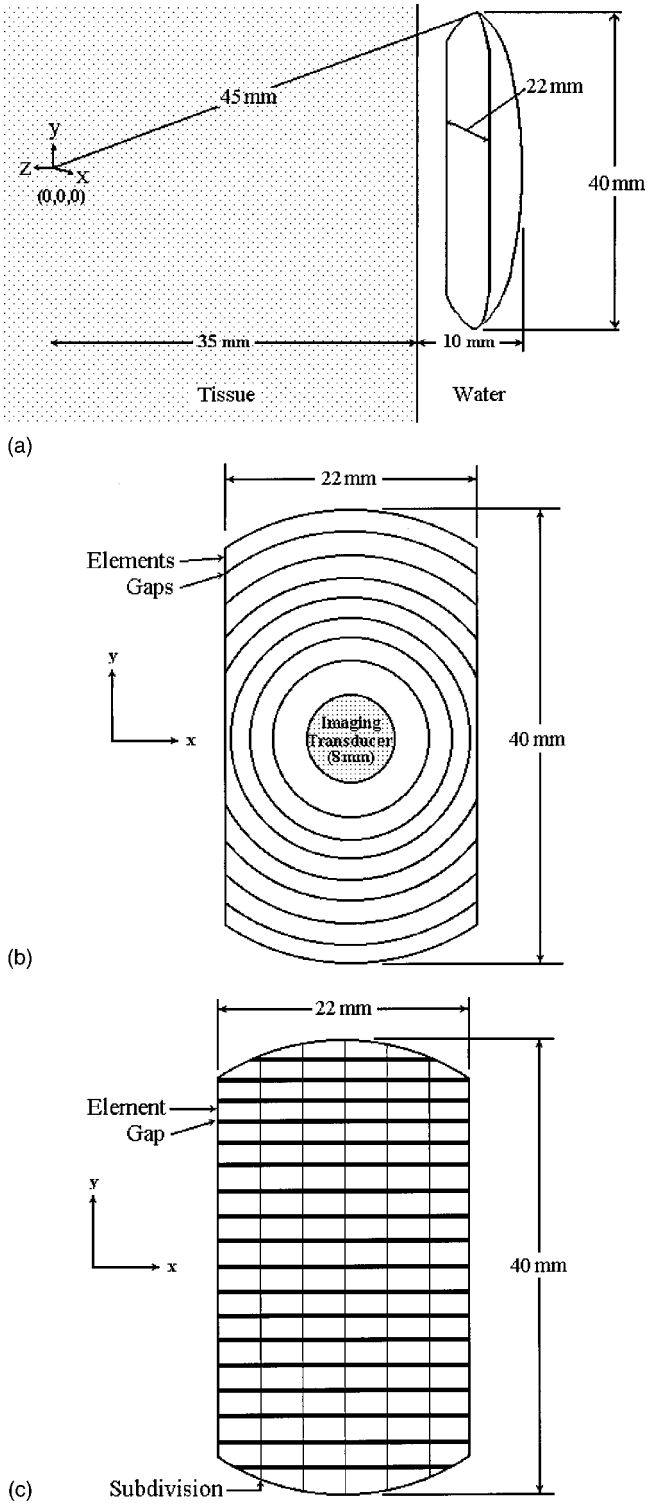

FIG. 1. (a) Truncated spherical array side view with water and tissue, (b) truncated spherical annular array front view, (c) truncated spherical linear array front view.

subelement of the source (x_s, y_s, z_s) (i.e., point radiator) to the field point being calculated, ΔA is the area of the subelement, and α is the attenuation coefficient. The simulations were run at a frequency of 4 MHz (see Table I for parameter values used), which has been shown to be appropriate for this depth of treatment.[42] The calculation requires that the dimensions of the subelements be small relative to a wavelength; in these simulations the subelements were modeled as squares with dimensions of a tenth of a wavelength on a side. Note that each element of the array was excited with equal amplitude, i.e., there was no apodization.

TABLE I. Properties used for the simulations, all at 4 MHz.

Material	Density (kg/m^3)	Speed (m/s)	Absorption coefficient (cm^{-1})
Water	1000	1500	0
Tissue	1000	1500	0.3224

Simulations were carried out with a 10 mm water standoff between the center of the array and a planar boundary with the tissue (at $z_{\text{Interface}} = -35$ mm), as shown in Fig. 1(a). Thus the origin of the coordinate system, located 45 mm from the center of the array, was separated from the center of the array by 10 mm of water, followed by 35 mm of tissue. For each point radiator-field point pair, the path in water and in tissue was calculated in order to account for the attenuation along the tissue portion of the path. The equation used to calculate the pressure field was thus modified:

$$p(x,y,z) \cong j \frac{\rho c k U_0 \Delta A}{2\pi} \sum_{\text{array surface}} \frac{e^{-[\alpha_W R_W + \alpha_T R_T + jkR_{\text{tot}}]}}{R_{\text{tot}}}, \qquad (2)$$

where α_W is the attenuation coefficient in water, α_T is the attenuation coefficient in tissue, R_W is the distance that the beam traveled through water, R_T is the distance that the beam traveled through tissue, and $R_{\text{tot}} = R_W + R_T$ is the total distance that the beam traveled along the straight line from source subelement to field point, see Fig. 1(a).

Since the intent of this study was the fundamental comparison of the performance of different array configurations, not all of the detailed aspects of the sound propagation were required. For example, the speed and density for both tissue and water were taken to be the same so that the analysis was not complicated by reflection and refraction. Additionally, the effects of nonlinear propagation were not incorporated to simplify the extensive and time consuming calculations of the fields. Studies that might be conducted in the future involving the calculation of temperature rise associated with the fields from these sources would need to consider nonlinear propagation.

The calculations were performed using programs written in Visual C++4.1 and executed on several Pentium-type personal computers. The fields were calculated for different cases of focal steering: no steering, steering -15 mm in the y direction (along the prostate), and steering -15 mm in the z direction (towards the transducer). The transducer element size (width) was varied. The array configurations and ranges of parameters examined are listed in Table II.

The performance of the arrays under each steering condition was assessed by first calculating the acoustic intensity at each field point, using the equation $I = p^2/2\rho c$, and then finding the ratio of intensity at the focus to the intensity of the largest unwanted lobe, G:

$$G = \frac{I_{\text{focus}}}{I_{\text{max,unwanted}}}. \qquad (3)$$

This G value provided a means to reduce the large amount of data contained in each calculated field to a single number to

TABLE II. Configurations and ranges of array parameters.

Array geometry	Element description	Element gap	Focal location(s)	Parameter(s) varied
TSA	Annular equal area	1/2 λ	(0,0,−15)	Number of elements: 6 to 14
TSL	Linear	1/2 λ	(0,0,0) (0,−15,0) (0,0,−15)	(a) Element width: 1 to 3 λ (b) Number of elements in *x*: 2, 4, 6, 12, 24
Cylindrical	Linear	1/2 λ	(0,0,0) (0,−15,0) (0,0,−15)	(a) Element width: 1 to 3 λ (b) Array length: 40, 50, or 60 mm
Curved cylindrical	Linear	1/2 λ	(0,0,0) (0,−15,0) (0,0,−15)	(a) Element width: 1 to 3 λ (b) Array length: 50 or 60 mm (c) Radius of array curvature: 50, 60, 75, or 90 mm

facilitate comparison among the numerous arrays and steering conditions. Although no thermal calculations were done as a part of this study, it is the authors' opinion that a *G* value of 4 or greater would be sufficient to prevent unintended damage to normal tissue, when used in conjunction with a properly planned therapy regimen and active rectal wall cooling.

The fields produced by the arrays were initially investigated at a low spatial resolution (1 mm=8/3 λ). This resulted in irregular (nonmonotonic) behavior of the *G* values as a function of the element size.[43] Since this phenomenon was discovered, simulations with higher spatial resolution (0.25 mm=2/3 λ) of the field have been performed, with the spatial resolution being limited by the practical consideration of simulation time. The results of these higher-resolution simulations did not show these irregularities and are presented here.

III. RESULTS AND DISCUSSION

A. Truncated spherical annular (TSA) array

The truncated spherical annular (TSA) array consisted of a truncated spherical shell divided into annular elements of equal area, with a gap λ/2 wide between adjacent elements. A center region of 8 mm diameter was considered inactive as it was reserved for an imaging transducer, see Fig. 1(b). The spherical shell had a 45 mm radius of curvature, with a face diameter of 40 mm which was truncated in the *x* direction to a width of 22 mm to allow passage through the rectum, as has been done for fixed focus transducers currently used by Focus Surgery, Inc.,[20] as well as in the studies by Curiel *et al.*[44] and Chapelon *et al.*[7] The spherical design, first proposed by Ebbini and Cain,[36] has the advantage of possessing a geometric focus, but the phase of signals applied to the transducer elements can be varied in order to steer the focus electronically from the geometric focus along the transducer axis, the *z* direction.

In Fig. 2 the results of steering to (0,0,−15) mm is shown for annular arrays containing various numbers of elements. An annular array of 6 annuli performed very poorly, the unwanted lobes in the field were numerous and almost the same intensity as the intended focus. An annular array of 8 annuli displayed improved performance, with a clearly discernable focus and a *G* value of 2.4. With 10 annuli, the *G* value increased to 5.7 (well above the $G>4$ criterion), which would provide adequate performance for clinical application.

Truncated spherical annular arrays with different dimensions and operating frequency were investigated earlier by Chapelon *et al.*[7] When the simulation parameters were modified to match those used by Chapelon *et al.*, the results agreed closely with theirs, supporting the validity of the present calculations.

B. Truncated spherical linear (TSL) array

The truncated spherical linear (TSL) array consisted of a truncated spherical shell transducer as used for the TSA array except that the transducer was divided into linear elements along the *y* direction with gaps (λ/2 width) between the elements, see Fig. 1(c). In addition, these linear elements were divided into six elements in the *x* direction, as indicated by the ''subdivision'' lines in the figure. This was required because, for these curved transducers, the appropriate phase

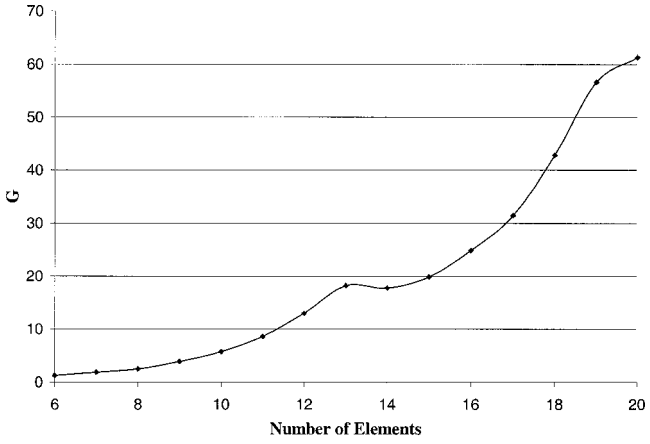

FIG. 2. Ratio of intensity at the focus to intensity of the maximum unwanted lobe versus number of elements for the annular array steered to (0,0,−15). Tissue was present and the gap between elements was 0.5 λ for all these calculations.

for steering also varies along the x direction. This study showed six elements in the x direction (symmetric elements in the $+$ and $-x$ directions have a common phase) were adequate for the steering desired and results shown are for this case only. This was the first design used to investigate the feasibility of focal steering in both the y and z directions.

Focal steering in the x direction was attempted using different numbers of subdivisions in the x direction (6, 12, and 24). The G values were extremely low even when 24 subdivisions were used (resulting in a very large number of elements in the array) and the beam could only be steered 5 mm off center. Based on these results, the current study was limited to examination of steering in only the y and z directions for all arrays studied.

Typical intensity field plots produced by the TSL array with an element width of λ are shown in the $y-z$ plane in Figs. 3(a)–3(c). When the array was focused at its geometric focus the unwanted lobe intensities were found to be much lower than the intensity at the focus (the G values were very large) as seen in Fig. 3(a). When the focus was steered to $(0,-15,0)$ mm, Fig. 3(b), significant unwanted lobes appeared, even for the smaller element widths (λ in this case). Better performance was obtained when steering to $(0,0,-15)$ mm; unwanted lobes can barely be seen in Fig. 3(c) The $x-z$ plane was also examined and it was found that unwanted grating lobes did appear as the array was steered in the z direction. However, these lobes were very close to the focus, so that they had the desirable effect of enlarging the focal region in this direction, which would decrease treatment time. Therefore, in the remainder of this paper the G value is based on an examination of unwanted lobes appearing in the $y-z$ plane.

Results in terms of the value for G versus the element width for the TSL array, unsteered and steered to $(0,-15,0)$ and $(0,0,-15)$ mm, are shown in Fig. 4. These results show that G decreased as the element width increased when the focus was steered away from the geometric focus. When the focus was not steered away from the geometric focus, (0,0,0) mm, the performance was superb, even at the larger element widths. In fact, the performance was approximately the same for all element widths examined. This makes sense since, when the specified focus coincided with the geometric focus, the array geometry dictated the focal position, and the phasing of the elements played no role. From the results for steering to $(0,0,-15)$ mm (i.e., decreasing the depth of the focus by 15 mm), it is apparent that the value for G was much greater than its value for steering the same distance in the y direction. The G value stayed above 7 for all element widths up to 3 λ, resulting in performance that was quite acceptable even at larger element widths. When steering to $(0,-15,0)$ mm, the value for G was low for all element widths, falling below 1 for element widths greater than about 1.6 λ, which was clearly unacceptable. Thus the performance of the TSL array was very poor when steered in the y direction, along the prostate, making it clearly unsuitable for steering in the $y-z$ plane.

A 1.5 D phased array of a similar form was investigated by Curiel *et al.*[44] Their array differed in dimensions and operating frequency, and, in the 1.5 D array, gaps were present between all of the elements except the central pairs, and all elements were of equal area. In agreement with this study, Curiel *et al.* concluded that having five elements in the x direction (achieved by combining the two middle elements of the TSL array into one) was necessary for adequate steering in the y and z directions, and did not attempt to steer in the x direction. However, their calculations differed from this

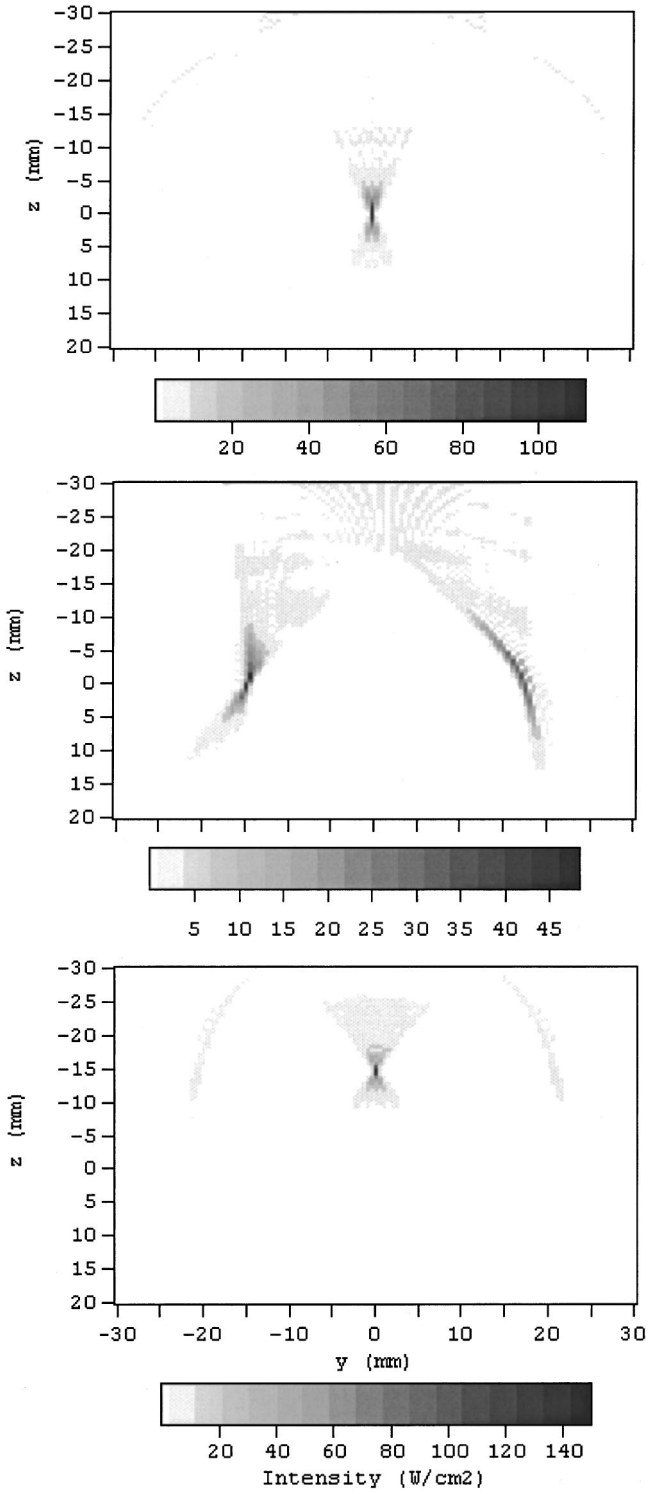

FIG. 3. Intensity as a function of field position for a TSL array with 1 λ wide elements, 0.5 λ gap between elements in the y direction, and 6 elements in the x direction. (a) With no steering; (b) steered to $(0,-15,0)$ mm, (c) steered to $(0,0,-15)$ mm.

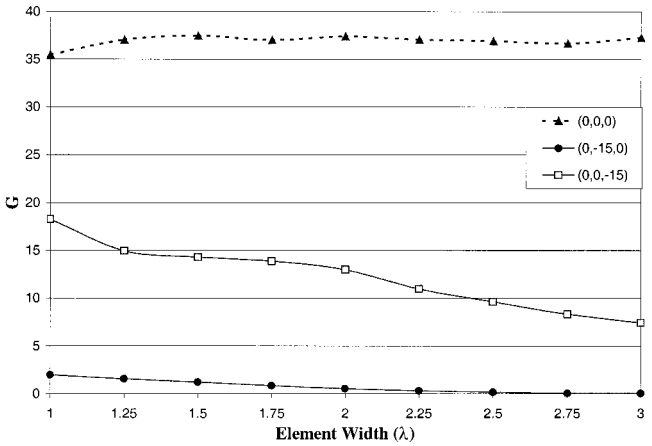

FIG. 4. *G* versus the element width for the TSL array focused at (0,0,0), (0,−15,0) mm, and (0,0,−15) mm.

study in that no tissue was included in their simulation, and the steering extremes were limited to 10 mm from the geometric focus. Another important difference was that they attempted to steer the focus deeper in the *z* direction than the geometric focus, whereas in this study it was found that the performance degraded rapidly when this was attempted. However, overall, the results obtained with the TSL array were in good agreement with their results.

C. Cylindrical array

The cylindrical array provided a line focus along the *y* direction. Note that the origin of the coordinate system for studies involving this array was located on the geometric line focus (i.e., 45 mm away from the center of the array in the *z* direction), and centered on the array in the *y* direction, see Fig. 5. The cylindrical array had a width of 22 mm to allow access through the rectum, and the length was varied from 40 mm to 60 mm. As with the TSL array, six elements were present along the *x* direction, as delineated by the ''subdivisions'' in the figure, in order to improve the focal steering.

Figure 6(a) shows that, for no steering, the value of *G* decreased steadily as the element width increased. The *G* value stayed above 4 for element widths of up to 1.75 λ. The use of larger array lengths appeared to have very little effect on *G* in this case, especially at larger element sizes, where the performance of arrays of different lengths was indistinguishable. In comparing these results to those obtained for the TSL array, the cylindrical array was seen to perform more poorly when the focus was not steered away from the origin. This was because, unlike a spherical array, the cylindrical array produced a geometric line focus rather than a point focus, and therefore required phasing of its elements in order to produce a point focus at the origin. This also led to the fact that the performance of the cylindrical array showed a definite dependence on element size.

The *G* values that resulted from steering the focus of the cylindrical array to (0,−15,0) mm are shown in Fig 6(b). In comparing these results to previous results obtained for the truncated spherical shell array (Fig. 4), the cylindrical array performed better when steered in the *y* direction, staying above 1 for all element widths examined. Furthermore, as the length of the array increased, there was a steady improvement in the performance of the cylindrical array. In fact, the *G* value stayed above 4 for the 60 mm arrays for element widths up to 1.75 λ.

However, the performance of the cylindrical array was much poorer than that for the truncated spherical linear array when steered in the *z* direction, see Fig. 6(c). This was due to the existence of much larger unwanted lobes than were exhibited for the truncated spherical arrays. Relative to earlier results with the TSL arrays (where $G>7$ for all element widths examined), the cylindrical shell displayed a drastic and disappointing decrease in performance when the focus was steered in the *z* direction. The *G* value fell below 4 for element widths greater than 1.5 λ. Increasing the length of the array appeared to provide only a minimal improvement in performance, which disappeared at larger element sizes.

Thus, it was found that the cylindrical array, while

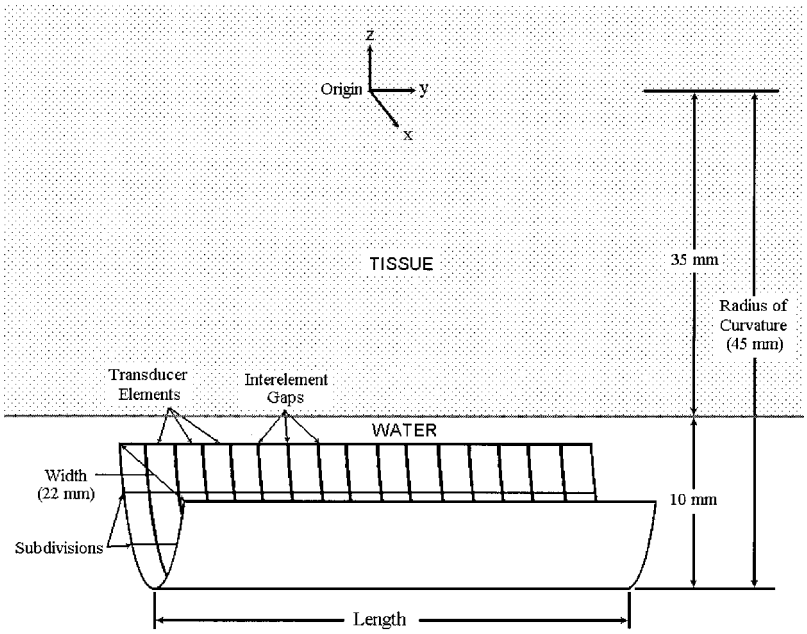

FIG. 5. Side view of cylindrical transducer array.

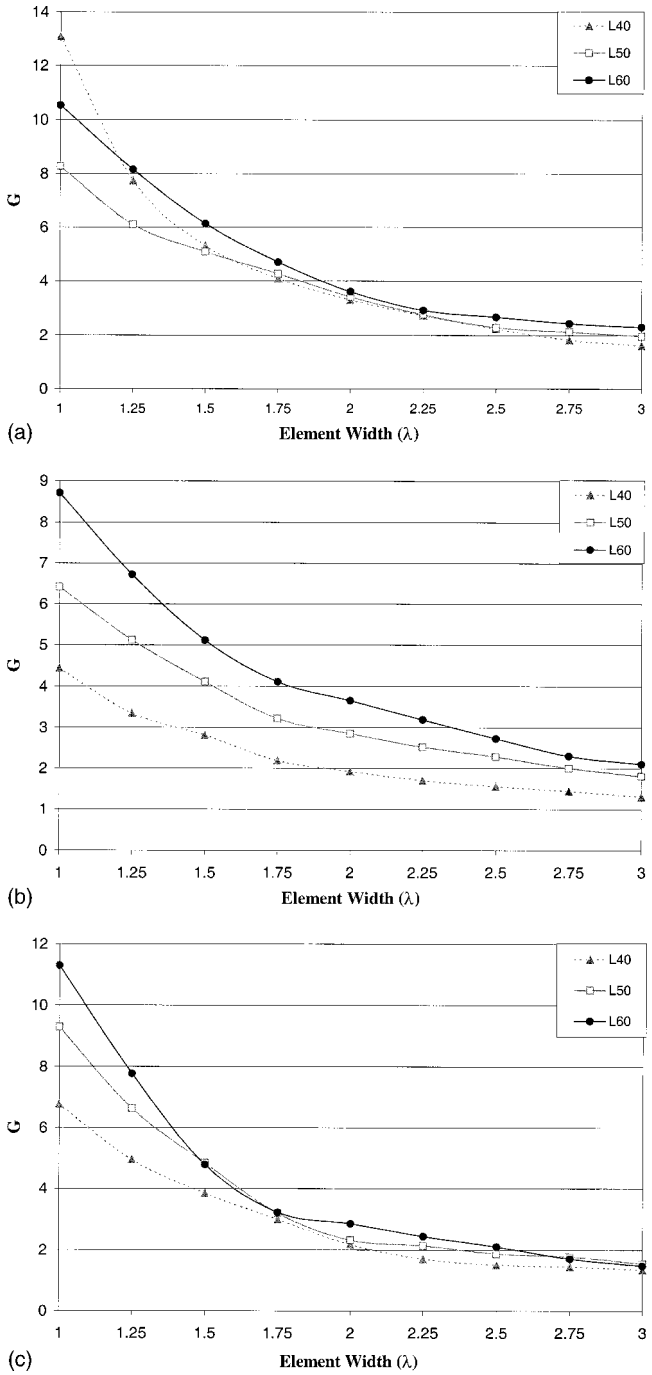

FIG. 6. *G* versus the element width for the cylindrical array with tissue present focused at (0,0,0) mm (a), (0,−15,0) mm (b), and (0,0,−15) mm (c).

showing some improvement in steering in the *y* direction, especially with increased array length, exhibited a drastic increase in the intensity level of unwanted lobes while steering in the *z* direction.

At this point, two transducer array geometries had been examined, which represented opposite extremes of a particular geometric spectrum. The spherical array, with equal curvature in the *x* and *y* directions, behaved poorly when steered in the *y* direction but performed well when steered in the *z* direction. On the other hand, the cylindrical array, which had no curvature in the *y* direction, exhibited improved behavior when steered in the *y* direction but performed much more poorly when steered in the *z* direction. The cylindrical array had the additional advantage that its length could be increased, improving its performance when steered in the *y* direction. Even though these results might have been expected, the present analysis shows just how much performance degrades for the particular array size and configuration.

D. Curved cylindrical (CC) array

The performance of a curved cylindrical (CC) array was examined as a compromise between the spherical and cylindrical arrays. This array, as shown in Fig. 7, was a cylindrical array that had curvature added in the *y* direction. When the radius of curvature of the CC array in the *y* direction equaled the radius of curvature in the *x* direction, the result was an array geometry similar to, but not exactly the same as, a truncated spherical array. With an infinite radius of curvature in the *y* direction, a cylindrical array was obtained. The effects on array performance of varying the radius of curvature in the *y* direction and the array length were investigated. The maximum length of the array was determined by the curvature in the *y* direction, since the ends of the array would eventually extend into the tissue, which was unacceptable. The smaller the radius of curvature, the shorter the maximum array length that could be used.

Figures 8(a)–(c) show the values for *G* as a function of element width, for curved cylindrical arrays for just one of the lengths investigated (50 mm) and for four different radii of curvature (50, 60, 75, and 90 mm). Note that the 50 mm radius of curvature corresponds to the greatest amount of curvature, most like a spherical array, while the 90 mm radius of curvature corresponds to a more gently curved, flatter array, most like a cylindrical array.

In Fig. 8(a), the *G* value is plotted against element width with the focus located at the origin, for 50 mm length arrays of varying curvature. As with the cylindrical array, since the curved cylindrical array lacked a geometric point focus, phasing of the elements was required for focusing at the origin, and therefore performance decreased with increasing element size. It is also apparent that performance (*G* value) decreased with increasing radius of curvature. Since the larger radius of curvature corresponded to a flatter array, these results agree quite well with the previous conclusion that the performance of the flat cylindrical array was inferior to that of the spherical array when the focus was located at the origin. Also, for the same radius of curvature, the *G* values for 60 mm length arrays (not shown in Fig. 8) were slightly lower than those for the 50 mm length arrays, showing a modest decrease in performance with increased array length. In comparing Fig. 8(a) with Fig. 6(a), there was a definite improvement in performance of the CC array over that of the cylindrical array, especially for arrays with shorter radii of curvature, whose performance exceeded even that of the TSL array for small element sizes. In all cases examined, the *G* value remained above 4, even for the largest element widths examined.

The results obtained when steering the curved cylindrical array to (0,−15,0) mm are shown in Fig. 8(b). There was a modest improvement in performance with increasing radius

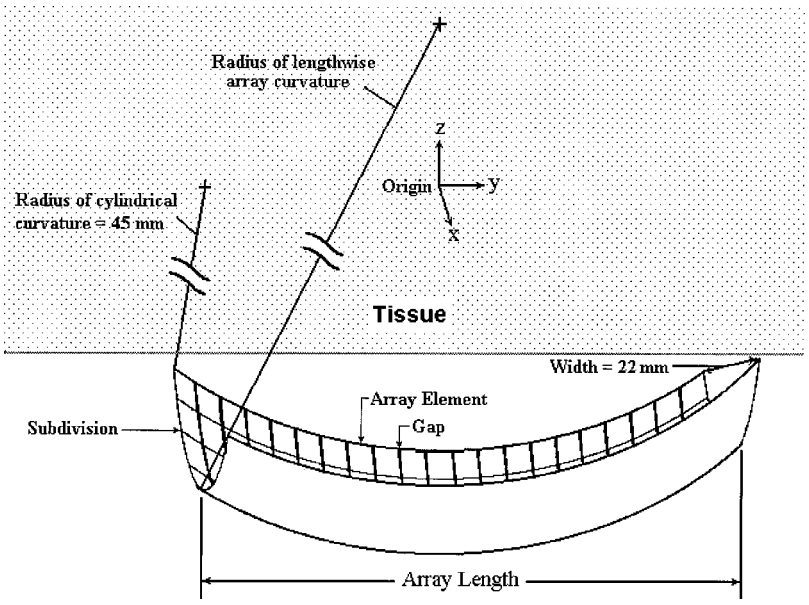

FIG. 7. Diagram of the curved cylindrical (CC) array.

of curvature. These results agreed with the conclusion that the flatter cylindrical array performed better than the truncated spherical array when steered to $(0,-15,0)$ mm. Also, the G values for the 60 mm array length curves, not shown, were higher than for the corresponding 50 mm array length curves, indicating improved performance with increased length, a characteristic which was also seen with the cylindrical array. Although the performance in all cases was not as good as with the cylindrical array of the same length, it was consistently better than that of the truncated spherical array, since G values stay above 1 for element widths as great as 2.25 λ. However, G values above 4 were obtained only for element widths less than 1.25 λ.

Figure 8(c) contains results obtained when the CC array was steered to $(0,0,-15)$ mm. Here, a trend opposite to that seen when steering in the y direction occurs. Performance generally decreased with increasing radius of curvature. These results agree quite well with the earlier conclusion that the spherical array performed better than the cylindrical array when steered in the z direction. Improved performance was obtained when the array length was increased from 50 mm to 60 mm [not shown in Fig. 8(c)], for the same radius of curvature. The performance in all cases was not nearly as good as with the truncated spherical arrays; however, it was consistently better than that of the cylindrical array, especially at larger element widths. In this case, G values above 4 can be achieved at all curvatures for element widths up to 2 λ.

IV. CONCLUSIONS

An analysis of the variation in G value with element size and geometry was conducted, with a G value greater than 4 as a cutoff for clinical applicability. The TSA array was able to electronically steer effectively in the z direction even with a small number of elements ($G>4$ for 10 elements). However, mechanical steering would still be required to move the focus in the x and y directions.

The TSL array was examined as a possible design to provide steering in the y and z directions. (Rotation of the array would still be necessary for steering in the x direction.) Like the TSA array, it was found to perform superbly when steered in the z direction. However, it performed poorly for steering in the y direction.

These results suggest that it is not possible to avoid mechanical steering of transducer arrays along the length of the prostate for transrectal treatment using the truncated spherical array geometry investigated. However, probe replacement during treatment to vary the depth of the focus can be eliminated from current treatments by using either the TSA or TSL arrays. The TSA array would be used for this purpose because it contains far fewer elements.

Results with the TSL array led to the consideration of using cylindrical arrays. The cylindrical array exhibited improved steering in the y direction, relative to the truncated spherical array. However, its performance when steered in the z direction was drastically reduced, relative to the truncated spherical array. Also, taking advantage of the ability to increase the length of the array improved results for y direction steering, and provided minimal improvement for z direction steering.

The curved cylindrical array was devised as a compromise, in order to take advantage of the best features of the spherical and cylindrical arrays. As hoped, the performance of the curved cylindrical array in all cases was between that of the truncated spherical array and the cylindrical array. Because of its variable curvature and length, the curved cylindrical array design may be optimized for steering in both the y and z directions.

In light of the $G>4$ criterion, it would appear that, of the geometries examined, both the 50 mm and 60 mm cylindrical arrays would satisfy this criterion for all focal steering cases examined with element widths as large as 1.5 λ. This was mainly due to superior performance when steering in the y direction, which was the worst steering scenario for the other two array geometries.

This study has investigated the effects of overall array geometry on array performance. In order to further improve the performance of the arrays, a number of other methods

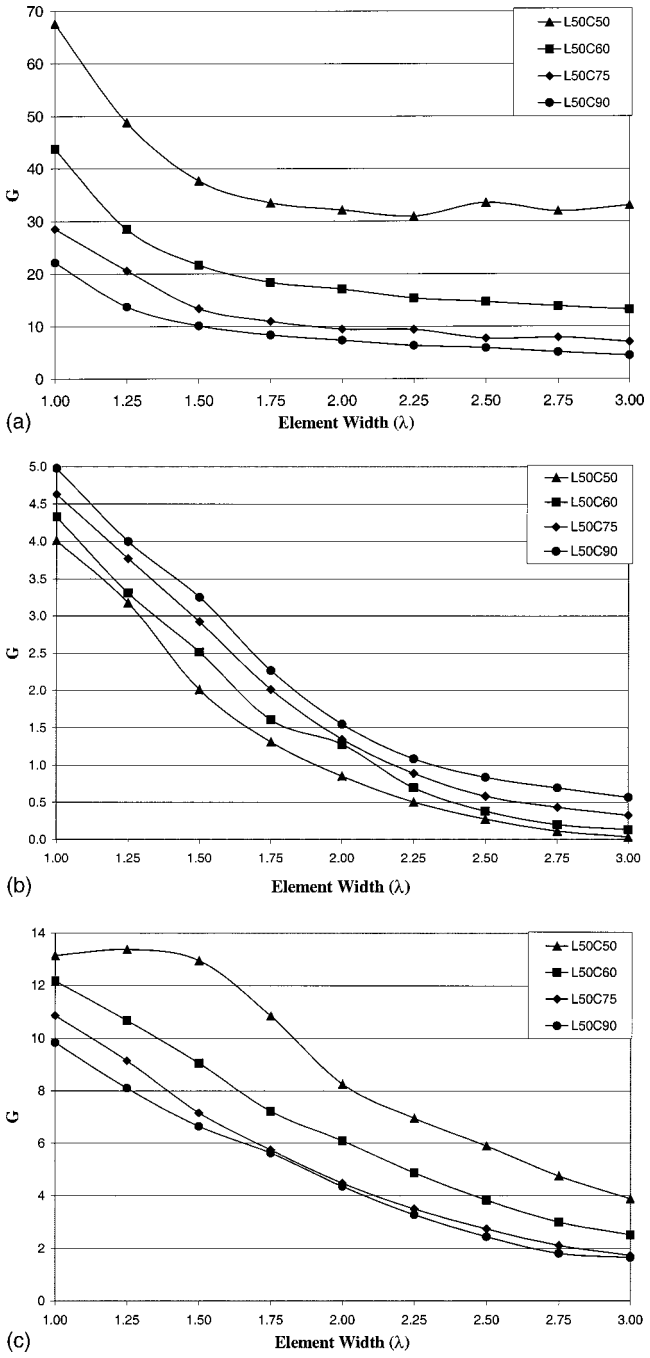

FIG. 8. *G* versus the element width for the CC array focused at (0,0,0) mm (a), (0,−15,0) mm (b), (0,0,−15) mm (c), with tissue present. Results are shown for a 50 mm length and different curvatures in the *y* direction.

may be employed. The randomization of element sizes may be used to decrease the intensity of unwanted lobes.[23] Use of only the portion of the array that contributes most directly to the intended focus can improve results by diminishing the amount of energy going into unwanted lobes.[32]

ACKNOWLEDGMENTS

The authors gratefully acknowledge help developing the early software by Rabin Pirakitti. This work was supported in part by U.S. Public Health Service Grants Nos. R43 CA 81340 and T32 CA 09067, awarded by the National Cancer Institute DHHS.

[1] A. Grove, ''Taking on prostate cancer,'' Fortune **133**, 54–56 (1996).
[2] L. Jaroff, ''The man's cancer,'' Time **147**, 58–65 (1996).
[3] J. Henkel, ''Prostate cancer: no one answer for testing or treatment,'' FDA Consum. **32**, 22–27 (1998).
[4] J. J. M. C. H. De la Rosette, F. C. H. D'ancona, and F. M. J. Debruyne, ''Current status of thermotherapy of the prostate,'' J. Urol. (Baltimore) **157**, 430–438 (1997).
[5] T. Parkins, ''Concern grows over prostate cancer treatment options,'' J. Natl. Cancer Inst. **86**, 897–898 (1994).
[6] T. R. Williams and N. Love, ''Treatment of localized prostate cancer,'' Postgrad Med. **100**, 105 (1996).
[7] J. Y. Chapelon, P. Faure, M. Plantier, D. Cathignol, R. Souchon, F. Gorry, and A. Gelet, ''The feasibility of tissue ablation using high intensity electronically focused ultrasound,'' Proc.-IEEE Ultrason. Symp., 1211–1214 (1993).
[8] F. L. Lizzi, ''High-precision thermotherapy for small lesions,'' Eur. Urol. **23**, 23–28 (1993).
[9] G. ter Haar, ''Ultrasound focal beam surgery,'' Ultrasound Med. Biol. **21**, 1089–1100 (1995).
[10] C. J. Diedrich and E. C. Burdette, ''Transurethral ultrasound array for prostate thermal therapy: initial studies,'' IEEE Trans. Ultrason. Ferroelectr. Freq. Control **UFFC-43**, 1011–1021 (1996).
[11] L. A. Frizzell, S. A. Goss, J. T. Kouzmanoff, and J. M. Yang, ''Sparse random ultrasound array for focal surgery,'' Proc.-IEEE Ultrasonics Symp. 1319–1323 (1996).
[12] S. A. Goss, L. A. Frizzell, J. T. Kouzmanoff, J. M. Barich, and J. M. Yang, ''Sparse random ultrasound phased array for focal surgery,'' IEEE Trans. Ultrason. Ferroelectr. Freq. Control **43**, 1111–1121 (1996).
[13] A. L. Malcolm and G. R. ter Haar, ''Ablation of tissue volumes using high intensity focused ultrasound,'' Ultrasound Med. Biol. **22**, 659–669 (1996).
[14] R. J. McGough, M. L. Kessler, E. S. Ebbini, and C. A. Cain, ''Treatment planning for hyperthermia with ultrasound phased arrays,'' IEEE Trans. Ultrason. Ferroelectr. Freq. Control **UFFC-43**, 1074–1084 (1996).
[15] I. H. Rivens, R. L. Clarke, and G. R. ter Haar, ''Design of focused ultrasound surgery transducers,'' IEEE Trans. Ultrason. Ferroelectr. Freq. Control **UFFC-43**, 1023–1031 (1996).
[16] N. T. Sanghvi, K. Hynynen, and F. L. Lizzi, ''New developments in therapeutic ultrasound,'' IEEE Eng. Med. Biol. Mag. **15**, 83–92 (1996).
[17] H. Wan, P. VanBaren, E. S. Ebbini, and C. A. Cain, ''Ultrasound surgery: comparison of strategies using phased array systems,'' IEEE Trans. Ultrason. Ferroelectr. Freq. Control **UFFC-43**, 1085–1097 (1996).
[18] F. Prat, J. Y. Chapelon, A. Arefiev, D. Cathignol, R. Souchon, and Y. Theilliere, ''High-intensity focused ultrasound transducers suitable for endoscopy: feasibility study in rabbits,'' Gastroint. Endoscop. **46**, 348–351 (1997).
[19] A. Gelet, J. Y. Chapelon, R. Bouvier, C. Pangaud, and Y. Lasne, ''Local control of prostate cancer by transrectal high intensity focused ultrasound therapy: preliminary results,'' J. Urol. (Baltimore) **161**, 156–162 (1999).
[20] N. T. Sanghvi, R. S. Foster, R. Bihrle, R. Casey, T. Uchida, M. H. Phillips, J. Syrus, A. V. Zaitsev, K. W. Marich, and F. J. Fry, ''Noninvasive surgery of prostate tissue by high intensity focused ultrasound: an updated report,'' Eur. J. Ultrasound **9**, 19–29 (1999).
[21] N. T. Sanghvi, R. S. Foster, F. J. Fry, R. Bihrle, C. Hennige, and L. V. Hennige, ''Ultrasound intracavity system for imaging, therapy planning and treatment of focal disease,'' Proc.-IEEE Ultrasonics Sym., 1249–1253 (1992).
[22] S. Madersbacher, M. Pedevilla, L. Vingers, M. Susani, and M. Marberger, ''Effect of high-intensity focused ultrasound on human prostate cancer in vivo,'' Cancer Res. **55**, 3346–3351 (1995).
[23] E. B. Hutchinson, M. T. Buchanan, and K. Hynynen, ''Design and optimization of an aperiodic ultrasound phased array for intracavitary prostate thermal therapies,'' Med. Phys. **23**, 767–776 (1996).
[24] E. B. Hutchinson and K. Hynynen, ''Intracavitary ultrasound phased arrays for noninvasive prostate surgery,'' IEEE Trans. Ultrason. Ferroelectr. Freq. Control **UFFC-43**, 1032–1042 (1996).
[25] J. Y. Chapelon, M. Ribault, F. Vernier, F. R. Souchon, and A. Gelet, ''Treatment of localised prostate cancer with transrectal high intensity focused ultrasound,'' Eur. J. Ultrasound **9**, 31–38 (1999).
[26] J. Y. Chapelon, J. Margonari, F. Vernier, F. Gorry, R. Ecochard, and A. Gelet, ''In vivo effects of high-intensity ultrasound on prostatic adenocarcinoma,'' Cancer Res. **52**, 6353–6357 (1992).
[27] G. O. Oosterhof, E. B. Cornel, G. A. Smits, F. M. Debruyne, and J. A.

Schalken, ''Influence of high-intensity focused ultrasound on the development of metastases,'' Eur. Urol. **32**, 91–95 (1997).
[28] A. Gelet, J. Y. Chapelon, J. Margonari, Y. Theillere, F. Gorry, D. Cathignol, and E. Blanc, ''Prostatic tissue destruction by high-intensity focused ultrasound: experimentation on canine prostate,'' J. Endourol. **7**, 249–253 (1993).
[29] C. Damianou and K. Hynynen, ''Focal spacing and near-field heating during pulsed high temperature ultrasound therapy,'' Ultrasound Med. Biol. **19**, 777–787 (1993).
[30] X. Fan and K. Hynynen, ''Ultrasound surgery using multiple sonications—treatment time considerations,'' Ultrasound Med. Biol. **22**, 471–482 (1996).
[31] E. S. Ebbini and C. A. Cain, ''Multiple-focus ultrasound phased-array pattern synthesis: optimal driving-signal distributions for hyperthermia,'' IEEE Trans. Ultrason. Ferroelectr. Freq. Control **UFFC-36**, 540–548 (1989).
[32] L. R. Gavrilov and J. W. Hand, ''Design and experimental evaluation of an endocavitary linear phased array for ultrasound surgery of prostate,'' Acoust. Phys. **46**, 144–152 (2000).
[33] L. R. Gavrilov and J. W. Hand, ''A theoretical assessment of the relative performance of spherical phased arrays for ultrasound surgery,'' IEEE Trans. Ultrason. Ferroelectr. Freq. Control **UFFC-47**, 125–139 (2000).
[34] C. A. Cain and S. Umemura, ''Concentric-ring and sector-vortex phased-array applicators for ultrasound hyperthermia,'' IEEE Trans. Microwave Theory Tech. **MTT-34**, 542–551 (1986).
[35] J. W. Hand, E. Ebbini, D. O'Keeffe, D. Israel, and S. Mohammadtaghi, ''An ultrasound linear array for use in intracavitary applicators for thermotherapy of prostatic diseases,'' Proc.-IEEE Ultrason. Symp., 1225–1228 (1993).
[36] E. S. Ebbini and C. A. Cain, ''A spherical-section ultrasound phased array applicator for deep localized hyperthermia,'' IEEE Trans. Biomed. Eng. **38**, 634–643 (1991).
[37] P. VanBaren, C. Simon, R. Seip, T. Solf, C. Cain, and E. Ebbini, ''Image-guided phased array system for ultrasound thermotherapy,'' Proc.-IEEE Ultrason. Symp., 1269–1272 (1996).
[38] M. Bechtold, B. Granz, H. P. Heindel, and K. Newerla, ''A linear phased array for prostate therapy,'' Proc.-IEEE Ultrason. Symp., 1385–1388 (1997).
[39] J. Zemanek, ''Beam behavior within the nearfield of the vibrating piston,'' J. Acoust. Soc. Am. **49**, 181–191 (1970).
[40] D. A. Hutchins, H. D. Mair, P. A. Puhach, and A. J. Osei, ''Continuous-wave pressure fields of utrasonic transducers,'' J. Acoust. Soc. Am. **18**, 1–12 (1986).
[41] K. B. Ocheltree and L. A. Frizzell, ''Sound field calculation for rectangular sources,'' IEEE Trans. Ultrason. Ferroelectr. Freq. Control **UFFC-36**, 242–248 (1989).
[42] N. T. Sanghvi, F. J. Fry, R. Bihrle, R. S. Foster, M. H. Phillips, J. Syrus, A. V. Zaitsev, and C. W. Hennige, ''Noninvasive surgery of prostate tissue by high-intensity focused ultrasound,'' IEEE Trans. Ultrason. Ferroelectr. Freq. Control **UFFC-43**, 1099–1110 (2000).
[43] J. S. Tan, L. A. Frizzell, N. T. Sanghvi, R. Seip, J. S. Wu, and J. T. Kouzmanoff, ''Design of focused ultrasound phased array for prostate treatment,'' Proc.-IEEE Ultrason. Symp., 1247–1251 (2000).
[44] L. Curiel, F. Chavrier, R. Souchon, A. Birer, and J. Y. Chapelon, ''1.5D multi-elements phased array applied to high intensity focused ultrasound,'' Proc.-IEEE Ultrason. Symp., 1451–1454 (1999).